2021 18th International Conference on Electrical Engineering, Computing Science and Automatic Control (CCE)
Mexico City, Mexico. November 10-12, 2021

Nonlinear Least Squares-based Identification of a Continuous Friction Model

Antonio Concha Sánchez
Faculty of Mechanical and Electrical Engineering
University of Colima
Colima, Mexico
aconcha@ucol.mx

Suresh Thenozhi
Faculty of Engineering
Autonomous University of Queretaro
Queretaro, Mexico
suresh@uaq.mx

***Abstract*—This paper presents an identification method to estimate the friction model parameters of a servomechanism. A continuously differentiable function is used to capture the friction effect. The velocity and friction force of the servo are estimated using an integral linear extended state observer (ILESO) that uses the position measurements. The nonlinear least squares (NLLS) method is used to identify the parameters of the nonlinearly parameterized friction model. Simulation studies comparing the identified continuous friction model with the classical discontinuous friction model and with a neural network-based friction model are presented.**

***Index Terms*—Extended state observer, friction identification, neural networks, nonlinear least squares.**

I. Introduction

The identification and compensation of the friction force is a fundamental design problem in high-performance motion control systems. To design an effective model-based friction compensator, a good knowledge of the friction model along with a precise identification scheme is required. However, it is hard to obtain an analytical description of the friction force. There exist different kinds of friction models and identification techniques for them [1]–[3]. The identified friction model can be incorporated into the control algorithm, whose performance depends on the accuracy of the estimated model.

The first step in friction identification is to obtain the friction force for a given velocity, which can be achieved using disturbance observers such as the high-gain observer [4], sliding mode observer [5], and nonlinear disturbance observer [6]. Meanwhile, an extended state observer can simultaneously estimate the system's states and friction without requiring an exact system model [7]–[11]. Its linear version, denoted as LESO, only has a single tuning parameter; therefore, it is widely used in friction estimation applications, using either the position measurements [7], [8] or their integral [12].

Using the estimated friction force and velocity, one can construct a fixed friction model. In the case of little or no theoretical knowledge of the friction model, a non-parametric model can be constructed using neural networks [13], fuzzy logic [14], or support vector machines [15]. Otherwise, a parametric friction model can be used, where its estimation accuracy depends on the nature of the friction model and its identification scheme.

The friction models are usually nonlinearly parameterized and can be either discontinuous or piecewise continuous; hence the ordinary LS algorithm is not suitable to identify them. Instead, a NLLS-based offline method can be used [16], [17]; however, improper choice of its initial parameters can lead to wrong parameter estimations. Moreover, discontinuous or piecewise continuous models can cause difficulties in the theoretical analysis and practical implementation, which can be overcome by incorporating continuous friction models in the compensation designs [7], [18]–[20]. However, improper choice of the friction parameters can lead to a significant approximation error at very low velocity. A comparative study of the continuous friction model with the discontinuous one could facilitate the parameter selection for the continuous model and the conversion between these models.

The aim of the paper is to identify the friction in a servomechanism represented using the continuous model proposed in [18]. Its parametric relationship with the classical discontinuous friction model [1] is theoretically established. The velocity and the friction force are estimated using an ILESO. It uses the integral of the servo's position to deal with the noise presented in the position measurements. A two-step offline identification scheme proposed in [21] is used to estimate those parameters. Firstly, the viscous and Coulomb coefficients of this friction model are estimated using the traditional LS method. Secondly, the NLLS is used to identify all the parameters of the friction model. The initial conditions of the NLLS are computed using both the parameters obtained in the first step and the parametric relations between the continuous and discontinuous friction models. Compared to the results presented in [21], this paper focuses on the comparison of the identified continuous friction model with the discontinuous one and with a neural network-based friction model. Finally, a proportional derivative (PD) controller with friction compensation is simulated to verify its performance by using the identified continuous model and the neural network model.

The rest of this paper is organized as follows. Section II presents the parametric relation between the continuous and discontinuous friction models. Section III discusses the ILESO-based estimation of the velocity and friction force. The identification of the continuous friction model is described in

978-1-6654-0029-9/21/$31.00

Section IV. Finally, Section V demonstrates simulation results, and Section VI concludes this paper.

II. Continuous Friction Model

Let us consider the widely used classical friction model [1] expressed by

$$F(\dot{q}) = (f_s - f_c)\exp^{-(|\dot{q}|/v_s)^m}\operatorname{sign}(\dot{q}) + f_c\operatorname{sign}(\dot{q}) + f_v\dot{q} \quad (1)$$

where F is the friction force, $\dot{q}$ is the velocity of the mechanical system, m is a parameter usually selected as 1 or 2, f_s is the stiction force, v_s is the Stribeck velocity, and f_c and f_v are the Coulomb and viscous friction coefficients, respectively. Note that this discontinuous model can bring complexity into the theoretical design of the controller due to its undifferentiable nature. On the other hand, a continuous friction model can greatly simplify the theoretical analysis but at the cost of approximation error.

A continuous friction model proposed in [18] is defined as

$$F(\dot{q}, \boldsymbol{\gamma}) = \gamma_1\left[\tanh(\gamma_2\dot{q}) - \tanh(\gamma_3\dot{q})\right] + \gamma_4\tanh(\gamma_5\dot{q}) + \gamma_6\dot{q} \quad (2)$$

where $\boldsymbol{\gamma} = [\gamma_1, \gamma_2, \ldots, \gamma_6]^{\mathrm{T}}$ is a vector of positive parameters. The term $[\tanh(\gamma_2\dot{q}) - \tanh(\gamma_3\dot{q})]$ captures the Stribeck effect, $\gamma_4\tanh(\gamma_5\dot{q})$ represents the Coulomb friction, $\gamma_6\dot{q}$ is the viscous friction, and $\gamma_1 + \gamma_4$ corresponds to the static friction coefficient.

To compare the friction models (1) and (2), first assume that $\gamma_5 \gg 0$, which produces $\tanh(\gamma_5\dot{q}) \approx \operatorname{sign}(\dot{q})$ and leads to the parameter relation $\gamma_4 = f_c$. Now, choosing $\gamma_6 = f_v$ we get

$$\gamma_4\tanh(\gamma_5\dot{q}) + \gamma_6\dot{q} \approx f_c\operatorname{sign}(\dot{q}) + f_v\dot{q} \quad (3)$$

Selecting $\gamma_1 = f_s - f_c$ implies that the remaining terms of the friction models must satisfy

$$\left[\tanh(\gamma_2\dot{q}) - \tanh(\gamma_3\dot{q})\right] \approx \underbrace{\exp^{-(|\dot{q}|/v_s)^m}\operatorname{sign}(\dot{q})}_{\sigma_2(\dot{q})} \quad (4)$$

which is equivalent to

$$\left[\frac{1-\exp^{-2\gamma_2\dot{q}}}{1+\exp^{-2\gamma_2\dot{q}}}\right] - \left[\frac{1-\exp^{-2\gamma_3\dot{q}}}{1+\exp^{-2\gamma_3\dot{q}}}\right] \approx \sigma_2(\dot{q}) \quad (5)$$

$$2\left[\frac{\exp^{-2\gamma_3\dot{q}} - \exp^{-2\gamma_2\dot{q}}}{(1+\exp^{-2\gamma_2\dot{q}})(1+\exp^{-2\gamma_3\dot{q}})}\right] \approx \sigma_2(\dot{q}) \quad (6)$$

Note that both sides of (6) have the same sign if and only if $\gamma_2 > \gamma_3$. Moreover, by choosing $\gamma_2 \gg 0$ leads to $\tanh(\gamma_2\dot{q}) \approx \operatorname{sign}(\dot{q})$ and converts (5) to

$$\underbrace{\frac{(1+\exp^{-2\gamma_3\dot{q}})\operatorname{sign}(\dot{q}) - (1-\exp^{-2\gamma_3\dot{q}})}{(1+\exp^{-2\gamma_3\dot{q}})}}_{\sigma_1(\dot{q})} \approx \sigma_2(\dot{q}) \quad (7)$$

where $(1+\exp^{-2\gamma_3\dot{q}})\operatorname{sign}(\dot{q}) - (1-\exp^{-2\gamma_3\dot{q}})$ equals to: $2\exp^{-2\gamma_3\dot{q}}$ for $\dot{q} > 0$; and -2 for $\dot{q} < 0$. Finally, if $\gamma_3 = 1/v_s$, then (7) is equivalent to

$$\begin{aligned} \frac{2\exp^{-2\gamma_3\dot{q}}}{(1+\exp^{-2\gamma_3\dot{q}})} &\approx \exp^{-(|\dot{q}|/v_s)^m} \quad \text{for } \dot{q} > 0, \\ \frac{-2}{(1+\exp^{-2\gamma_3\dot{q}})} &\approx -\exp^{-(|\dot{q}|/v_s)^m} \quad \text{for } \dot{q} < 0. \end{aligned} \quad (8)$$

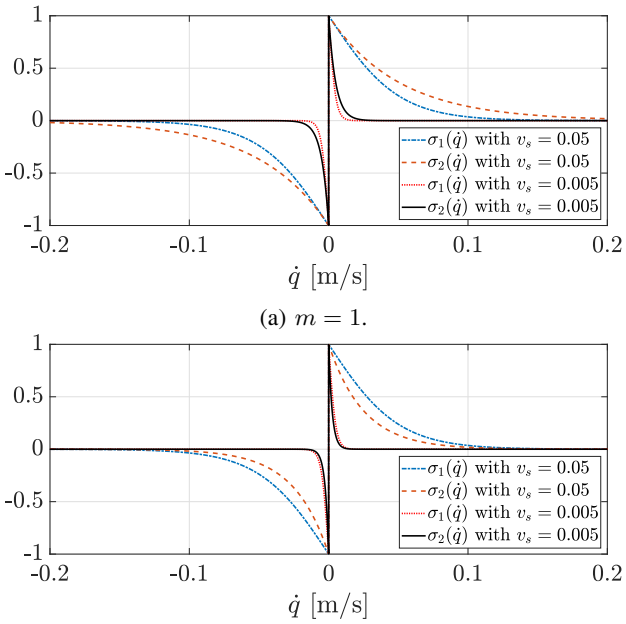

(a) $m = 1$.

(b) $m = 2$.

Fig. 1: Comparison of $\sigma_1(\dot{q})$ and $\sigma_2(\dot{q})$.

Note that the values of Stribeck velocity depends upon the mechanism and lubricant, and typically varies between the range 0.00001 and $0.1\,\mathrm{m/s}$ [1]. The approximation (8) is satisfied for these typical values of v_s. The comparison of the functions $\sigma_1(\dot{q})$ and $\sigma_2(\dot{q})$ using the parameter m equals to 1 and 2, is shown in Fig. 1, which indicates that $\sigma_1(\dot{q}) \approx \sigma_2(\dot{q})$.

From the above analysis, it can be concluded that the continuous model represented in (2) behaves similarly to the classical model in (1) if

$$\gamma_5 \gg 0, \quad \gamma_2 > \gamma_3, \quad \gamma_2 \gg 0 \quad (9)$$

and

$$\gamma_4 = f_c, \quad \gamma_6 = f_v, \quad \gamma_1 = f_s - f_c, \quad \gamma_3 = 1/v_s. \quad (10)$$

III. Observer design for Velocity and Friction Estimation

Let us consider the following servomechanism model with the nonlinear continuous friction force (2)

$$\begin{aligned} \ddot{q} + aF(\dot{q}, \boldsymbol{\gamma}) &= bu \\ y &= q + d \end{aligned} \quad (11)$$

where a and b are known positive parameters, with a being dependent on the inertia or mass of the servo, and b is proportional to the gain of the servo amplifier. Moreover, u is the control input and y is the measured output, that is the servo position q corrupted by an additive bounded noise d. By letting $x_1 = q$ and $x_2 = \dot{q}$, and introducing the new extended state variables $x_0 = \int_0^t y(\tau)\mathrm{d}\tau$ and $x_3 = -aF(\dot{q}, \boldsymbol{\gamma})$, as well as their dynamics $\dot{x}_0 = x_1 + d$ and $\dot{x}_3 = -a\dot{F}(\dot{q}, \boldsymbol{\gamma})$, the

overall dynamics of the servomechanism can be reformulated as the following state-space representation:

$$\frac{\mathrm{d}}{\mathrm{d}t}\begin{bmatrix} x_0 \\ x_1 \\ x_2 \\ x_3 \end{bmatrix} = \begin{bmatrix} 0 & 1 & 0 & 0 \\ 0 & 0 & 1 & 0 \\ 0 & 0 & 0 & 1 \\ 0 & 0 & 0 & 0 \end{bmatrix}\begin{bmatrix} x_0 \\ x_1 \\ x_2 \\ x_3 \end{bmatrix} + \begin{bmatrix} d \\ 0 \\ bu \\ -a\dot{F} \end{bmatrix} \quad (12)$$

where the term $\dot{F}$ is bounded since the friction force F represented using (2) is a continuous function of $\dot{q}$. Now, consider the following ILESO corresponding to system (12)

$$\frac{\mathrm{d}}{\mathrm{d}t}\begin{bmatrix} \widehat{x}_0 \\ \widehat{x}_1 \\ \widehat{x}_2 \\ \widehat{x}_3 \end{bmatrix} = \begin{bmatrix} 4\theta\,(x_0 - \widehat{x}_0) + \widehat{x}_1 \\ 6\theta^2\,(x_0 - \widehat{x}_0) + \widehat{x}_2 \\ 4\theta^3\,(x_0 - \widehat{x}_0) + \widehat{x}_3 \\ \theta^4\,(x_0 - \widehat{x}_0) \end{bmatrix} + \begin{bmatrix} 0 \\ 0 \\ bu \\ 0 \end{bmatrix} \quad (13)$$

where θ is the observer gain that represents its bandwidth. Using (12) and (13), the error dynamics of the system is obtained as

$$\frac{\mathrm{d}}{\mathrm{d}t}\begin{bmatrix} e_0 \\ e_1 \\ e_2 \\ e_3 \end{bmatrix} = \underbrace{\begin{bmatrix} -4\theta & 1 & 0 & 0 \\ -6\theta^2 & 0 & 1 & 0 \\ -4\theta^3 & 0 & 0 & 1 \\ -\theta^4 & 0 & 0 & 0 \end{bmatrix}}_{\mathbf{A}}\underbrace{\begin{bmatrix} e_0 \\ e_1 \\ e_2 \\ e_3 \end{bmatrix}}_{\mathbf{e}} + \underbrace{\begin{bmatrix} d \\ 0 \\ 0 \\ -a\dot{F} \end{bmatrix}}_{\mathbf{\Lambda}} \quad (14)$$

where $e_i = x_i - \widehat{x}_i$, $i = 0, 1, 2, 3$ are the state estimation errors. Since $\mathbf{A}$ is Hurwitz and the disturbance vector $\mathbf{\Lambda}$ is bounded, i.e., $\|\mathbf{\Lambda}\| \leq \overline{\Lambda}$, then the estimation error $\mathbf{e}$ in (14) fulfills the following inequality

$$\|\mathbf{e}(t)\| \leq \alpha \exp^{-\beta(t-t_o)}\left[\|\mathbf{e}(t_0)\| - \frac{\overline{\Lambda}}{\beta}\right] + \frac{\mu\overline{\Lambda}}{\beta}, \quad t \geq t_0 \quad (15)$$

where $\alpha > 0$, and $\beta > 0$ is a parameter proportional to θ. The above inequality implies that the estimated states $\widehat{x}_i$, $i = 0, 1, 2, 3$ exponentially converge to a bounded ball around the system states x_i [21].

The identification procedure is carried out in closed-loop by means of the following Proportional Derivative (PD) controller

$$u = \ddot{x}_d + k_d(\dot{x}_d - \widehat{x}_2) + k_p(x_d - \widehat{x}_1) \quad (16)$$

where $\widehat{x}_1$ and $\widehat{x}_2$ are obtained using the ILESO, and $x_d, \dot{x}_d, \ddot{x}_d$ are the desired position, velocity, and acceleration input references, respectively.

IV. Identification of the Continuous Friction Model

A two-step offline estimation procedure, described in [21], is used to obtain the parameters γ_i, $i = 1, 2, \ldots, 6$ of the continuous friction model $F(\dot{q}, \boldsymbol{\gamma})$ in (2) using the estimated friction force $\widehat{F} = -\widehat{x}_3/a$ and velocity $\widehat{x}_2$ produced by the ILESO. In the first step, the parameters γ_4 and γ_6 are identified through the offline LS algorithm. The second step uses these identified parameters, and exploits assumptions in (9) and the parametric relations in (10) to provide a good initial guess for the NLLS method, which iteratively searches the best estimate $\widehat{\boldsymbol{\gamma}}$ for the parameter vector $\boldsymbol{\gamma}$ of the continuous friction model (2). The block diagram representation of the identification scheme is provided in Fig. 2, and its details are described below.

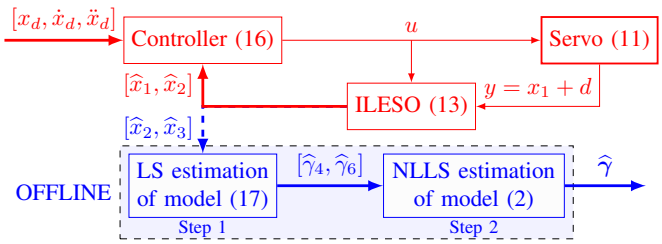

Fig. 2: Block diagram of the identification scheme.

A. LS method

To apply the LS method, the friction model need to be linearly parameterized. For that, the Stribeck effect is assumed to be zero in the friction models (1) and (2). This leads to the parametric relations $\gamma_4 = f_c$ and $\gamma_6 = f_v$, hence

$$\widehat{F}(t) = \gamma_4 \mathrm{sign}(\widehat{x}_2(t)) + \gamma_6 \widehat{x}_2(t) = \boldsymbol{\psi}^{\mathrm{T}}(t)\boldsymbol{\vartheta} \quad (17)$$

where $\boldsymbol{\psi}(t) = [\mathrm{sign}(\widehat{x}_2(t)), \widehat{x}_2(t)]^{\mathrm{T}}$ and $\boldsymbol{\vartheta} = [\gamma_4, \gamma_6]^{\mathrm{T}}$. The above linear parameterized model can be now identified by means of the LS method by minimizing the following cost function:

$$V_1(\widehat{\boldsymbol{\vartheta}}) = \frac{1}{N}\sum_{k=1}^{N}\left[\widehat{F}(k) - (\widehat{\gamma}_4 \mathrm{sign}(\widehat{x}_2(k)) + \widehat{\gamma}_6 \widehat{x}_2(k))\right]^2 \quad (18)$$

where the vector $\widehat{\boldsymbol{\vartheta}} = [\widehat{\gamma}_4, \widehat{\gamma}_6]^{\mathrm{T}}$ is an estimate of $\boldsymbol{\vartheta}$, and N is the number of samples of $\widehat{F}$ and $\widehat{x}_2$, which are obtained at every sampling period T_s. Vector $\widehat{\boldsymbol{\vartheta}}$ is given by [22]

$$\widehat{\boldsymbol{\vartheta}} = \left[\sum_{k=1}^{N}\boldsymbol{\psi}(k)\boldsymbol{\psi}^{\mathrm{T}}(k)\right]^{-1}\left[\sum_{k=1}^{N}\boldsymbol{\psi}(k)\widehat{F}(k)\right] \quad (19)$$

provided that this inverse matrix exists, which is guaranteed if the servomechanism input u is persistently exciting, i.e., it has a rich spectrum. As a rule of thumb, r sinusoids with different frequencies in the input signal u permits estimating $2r$ parameters [23]. Since, the continuous friction model $F(\dot{q}, \boldsymbol{\gamma})$ in (2) has 6 parameters, the control input u should have at least 3 different frequencies.

B. NLLS method

The parameters $\gamma_1, \ldots, \gamma_6$ of the nonlinearly parameterized continuous friction model in (2) are identified through the NLLS method by minimizing the following performance index:

$$V_2(\widehat{\boldsymbol{\gamma}}) = \frac{1}{N}\sum_{k=1}^{N}[\widehat{F}(k) - (\widehat{\gamma}_4 \tanh(\widehat{\gamma}_5 \widehat{x}_2(k)) + \widehat{\gamma}_6 \widehat{x}_2(k) + \widehat{\gamma}_1[\tanh(\widehat{\gamma}_2 \widehat{x}_2(k)) - \tanh(\widehat{\gamma}_3 \widehat{x}_2(k))])]^2 \quad (20)$$

where $\widehat{\boldsymbol{\gamma}} = [\widehat{\gamma}_1, \widehat{\gamma}_2, \ldots, \widehat{\gamma}_6]^{\mathrm{T}}$ is an estimate of $\boldsymbol{\gamma}$.

Compared to the convex cost function $V_1(\widehat{\boldsymbol{\vartheta}})$ of the LS method that has the solution $\widehat{\boldsymbol{\vartheta}}$ in (19), it is not possible to find an analytical solution to the vector estimate $\widehat{\boldsymbol{\gamma}}$ using the NLLS method. Therefore, the NLLS method uses the trust-region-reflective iterative algorithm [24] to find the estimate $\widehat{\boldsymbol{\gamma}}$. This algorithm is based on the interior-reflective Newton method and generates strictly feasible iterates by using an affine scaling transformation and following piecewise linear paths, called as reflection paths. However, the estimation accuracy of this parameter depends on its initial value $\widehat{\boldsymbol{\gamma}}(0)$, where the convergence to the global optimum that minimizes V_2 in (20) is assured if the initial guess $\widehat{\boldsymbol{\gamma}}(0)$ is close to this optimum [22]. This can be guaranteed by choosing the parameters $\widehat{\gamma}_i(0)$, $i = 1, 2, \ldots, 6$ of the vector $\widehat{\boldsymbol{\gamma}}(0)$ based on the identification scheme described in the next paragraph.

First, the estimates $\widehat{\gamma}_4$ and $\widehat{\gamma}_6$, previously obtained using the LS method, are used as the initial values $\widehat{\gamma}_4(0)$ and $\widehat{\gamma}_6(0)$ for the NLLS. Now, by using the first and third parameter relations in (10) we obtain $\widehat{\gamma}_1 = \hat{f}_s - \widehat{\gamma}_4$, where it is recommended to select $\hat{f}_s = \kappa\widehat{\gamma}_4$, with $\kappa \in [1.2, 1.5]$. Thus, the parameter $\widehat{\gamma}_1$ is initialized as $\widehat{\gamma}_1(0) = [\kappa - 1]\widehat{\gamma}_4(0)$. In order to satisfy the first and third inequalities in (9), larger initial values for $\widehat{\gamma}_2$ and $\widehat{\gamma}_5$ are needed. Initial values $\widehat{\gamma}_2(0)$ and $\widehat{\gamma}_5(0)$ between 100 and 300 are recommended. Finally, the initial value for $\widehat{\gamma}_3$ can be chosen such that it satisfies the second inequality in (9). An initial value of $\widehat{\gamma}_3(0) = \widehat{\gamma}_2(0)/3$ is recommended.

V. Results and Discussion

This section presents numerical simulations to validate the identified friction model. All the simulation studies are performed in the Matlab software with the Dormant-Prince numerical integration solver at a sampling period of 1 ms.

First, we compare the continuous and discontinuous friction models. For that, we choose the parameters of the model (2) as $\boldsymbol{\gamma} = [10, 700, 50, 5, 700, 50]^{\mathrm{T}}$, where the unit for γ_1 and γ_4 is N, for γ_2, γ_3, and γ_5 is s/m, and for γ_6 is Nm/s. Now, using the parametric relations in (10) leads to the parameters $f_s = 15\,\mathrm{N}, f_c = 5\,\mathrm{N}, f_v = 50\,\mathrm{Nm/s}$, and $v_s = 0.02\,\mathrm{m/s}$ of (1). The resulting friction curves of these models are shown in Fig. 3, which corroborates that the continuous model in (2) behaves similarly to the classical discontinuous model in (1).

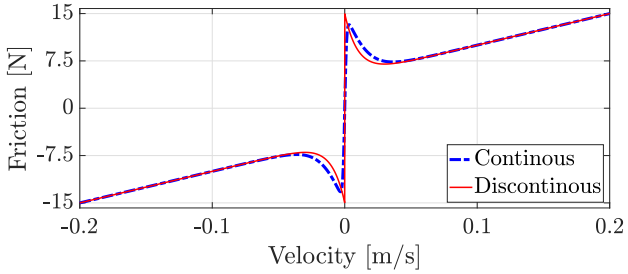

Fig. 3: Comparison of the continuous and discontinuous friction curves.

Now, let us consider the servo system (11) with $a = 0.14\,\mathrm{kg}^{-1}$, $b = 1.5\,\mathrm{m/(s^2V)}$, and the nominal friction coefficients of (2) are chosen to be $\boldsymbol{\gamma} = [7, 277, 100, 5.92, 200.6, 150]^{\mathrm{T}}$. The ILESO in (13) with the gain $\theta = 1000$ and the PD controller (16) with $k_p = 200$ and $k_d = 120$ are used here to obtain the signals $\widehat{F}$ and $\widehat{x}_2$, as described in Fig. 2. To provide a rich spectrum for the identification, we choose

$$x_d(t) = 0.0015\,[\sin(\pi t) + 2\sin(1.4\pi t) + 3\sin(2\pi t) + \sin(4\pi t) + \sin(6\pi t)] \quad [\mathrm{m}] \tag{21}$$

To show the robustness of the ILESO, a random measurement noise d is added to x_1. The resulting estimation of the position, velocity, and friction from the ILESO is compared with their actual values, see Fig. 4. The results show a good estimation, especially for the position state.

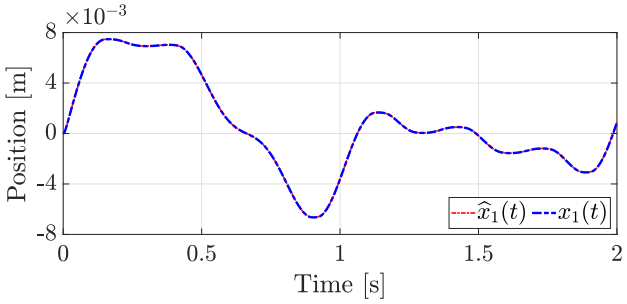

(a) Position.

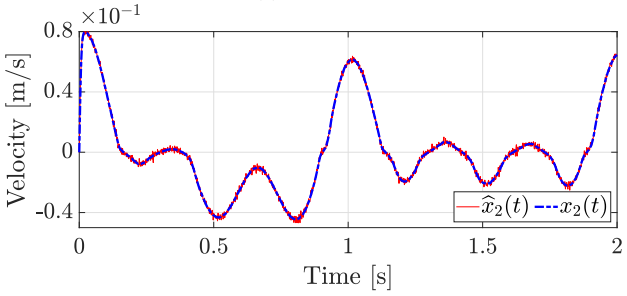

(b) Velocity.

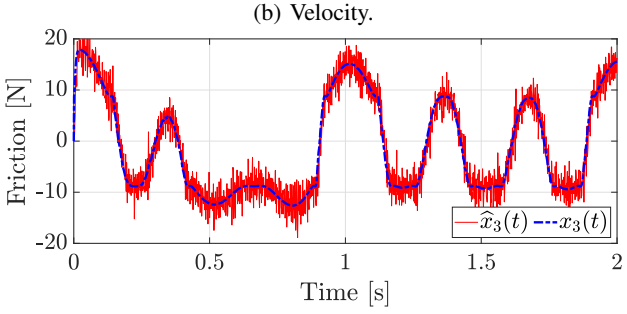

(c) Friction.

Fig. 4: Estimations obtained using the ILESO.

The first step of the identification method produces the estimates $\widehat{\gamma}_4 = 5.46$ and $\widehat{\gamma}_6 = 164.27$, which are used to obtain the initial conditions for the second step of our identification technique. By choosing the initial condition vector as $\widehat{\boldsymbol{\gamma}}(0) = [2.73, 230, 76.67, 5.46, 230, 164.27]^{\mathrm{T}}$, the NLLS method produces the estimated vector $\widehat{\boldsymbol{\gamma}} =$

$[6.40, 260.02, 95.39, 5.93, 200.28, 149.01]^{\mathrm{T}}$ of the following offline model

$$\begin{aligned}\widehat{F}_{\mathrm{NL}} =&\widehat{\gamma}_1 \left[\tanh\left(\widehat{\gamma}_2 \widehat{x}_2\right) - \tanh\left(\widehat{\gamma}_3 \widehat{x}_2\right)\right] \\ &+ \widehat{\gamma}_4 \tanh\left(\widehat{\gamma}_5 \widehat{x}_2\right) + \widehat{\gamma}_6 \widehat{x}_2 \end{aligned} \tag{22}$$

The resulting parameter estimation error vector is $\widetilde{\boldsymbol{\gamma}} = \boldsymbol{\gamma} - \widehat{\boldsymbol{\gamma}} = [0.60, 16.98, 4.61, -0.01, 0.32, 0.99]^{\mathrm{T}}$. It is possible to appreciate that all the estimates are close to their nominal values. Fig. 5(a) compares the friction force curves of the actual friction force F and its estimate $\widehat{F}_{\mathrm{NL}}$, which shows that $\widehat{F}_{\mathrm{NL}}$ precisely approximates F.

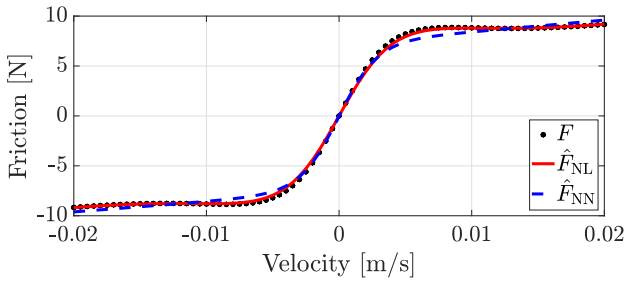

(a) Friction curves.

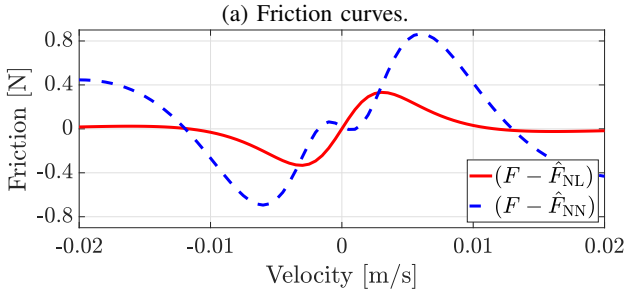

(b) Estimation error.

Fig. 5: Comparison of the estimated friction models.

Finally, the identified continuous friction model is compared with a neural network-based non-parametric identification technique [25]. For that, a feed-forward neural network with one hidden layer is used to estimate the continuous-friction model. For a given input $\widehat{x}_2$, the corresponding network output is

$$\widehat{F}_{\mathrm{NN}} = \mathbf{w}^{\mathrm{T}} \boldsymbol{\phi}(\widehat{x}_2) + w_0 \tag{23}$$

where $\widehat{F}_{\mathrm{NN}}$ is the friction force estimated by the neural network, $\mathbf{w} = [w_1, w_2, ..., w_l] \in \mathbb{R}^l$ and $\boldsymbol{\phi} = [\phi_1, \phi_2, ..., \phi_l] \in \mathbb{R}^l$ are the weights and activation function vectors, respectively, with l as the number of hidden neurons, and w_0 is the bias. Since the friction model (2) consists of hyperbolic tangent functions, the activation of the neurons is modeled with this kind of function, which has the following expression:

$$\phi(\widehat{x}_2) = \frac{2}{1 + \exp^{-2\widehat{x}_2}} - 1 = \tanh(\widehat{x}_2) \tag{24}$$

The Levenberg-Marquardt (LM) algorithm is used to train the network. It updates the network parameters $\mathbf{w}$ and w_0 in an iterative manner to minimize the following cost function, which is based on the estimation error of friction force for M training samples.

$$V_3(\mathbf{w}, w_0) = \frac{1}{M} \sum_{k=1}^{M} \left[\widehat{F}(k) - \widehat{F}_{\mathrm{NN}}(k)\right]^2 \tag{25}$$

where $\widehat{F} = -\widehat{x}_3/a$ is obtained from the ILESO. Moreover, $\widehat{F}_{\mathrm{NN}}$ uses the velocity estimations from the ILESO.

The number of hidden neurons is set as $l = 10$ and the neural network is trained at a learning rate of 0.05 using $M = 2000$ training samples. The resulting friction curve $\widehat{F}_{\mathrm{NN}}$ is shown in Fig. 5(a). Fig. 5(b) shows the friction estimation error produced by both the continuous and neural network friction models. It indicates that the error produced by the former is slightly smaller than that of the latter. However, the accuracy of neural network-based model $\widehat{F}_{\mathrm{NN}}$ can be improved by increasing its number of hidden neurons l.

Remark 1. *Both the LM and trust region algorithms are Newton methods and exhibit quadratic speed of convergence near to the optimum. However, if the solution is far away from the optimum, LM algorithms slow down their speed dramatically. In contrast, the trust region methods overcome this problem by increasing their step size, and they quickly move to a neighborhood around the global optimum [26].*

A. Validation of the identified friction model

To further investigate the effectiveness of the identified offline friction models, they are employed to compensate the friction by incorporating it to the PD controller (16). The resulting control law is given by

$$u = \ddot{x}_d + k_d(\dot{x}_d - \widehat{x}_2) + k_p(x_d - \widehat{x}_1) + a\widehat{F}_{\mathrm{N}} \tag{26}$$

where $\widehat{F}_{\mathrm{N}}$ uses either the $\widehat{F}_{\mathrm{NL}}$ in (22) or the $\widehat{F}_{\mathrm{NN}}$ in (23).

Same control gains are used in the controller (26), i.e., $k_p = 200$ and $k_d = 120$, whereas a smaller observer gain $\theta = 200$ is employed to reduce the noise sensitivity of the controller. The resulting position tracking performance is shown in Fig. 6(a). The position tracking errors $\epsilon_1 = (x_1 - x_d)$ produced by the controller (26) based on $\widehat{F}_{\mathrm{NL}}$ and $\widehat{F}_{\mathrm{NN}}$ are compared in Fig. 6(b), and their root mean square error (RMSE) values are 6.73×10^{-4} and 6.92×10^{-4}, respectively. In the absence of the friction compensation term, i.e., applying the controller (16), the RMSE value of ϵ_1 is 11.95×10^{-4}. These results indicate that the controller based on the continuous friction model produces a small tracking error, hence validating its accuracy.

VI. Conclusion

In this paper, the offline identification method in [21] is applied for estimating the parameters of a continuous friction model. The identification method uses the velocity and friction estimations from the ILESO. This identified continuous friction model was compared with the classical discontinuous friction model and with a feed-forward neural network friction model. Moreover, the continuous friction model and the one

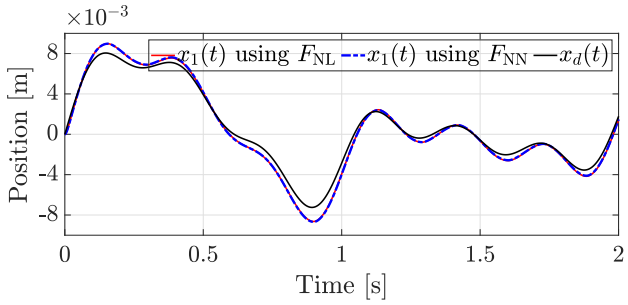

(a) Position.

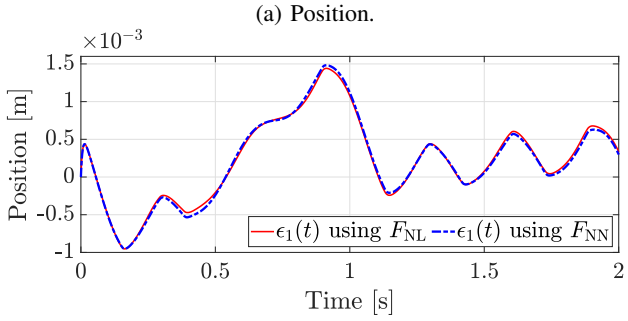

(b) Position error.

Fig. 6: Comparison of the position tracking performance.

based on the neural network are incorporated in a PD controller with friction compensation. The results indicated that the continuous model produces a smaller tracking error than the model estimated with the neural network.

REFERENCES

[1] B. Armstrong-Hélouvry, P. Dupont, and C. C. De Wit, "A survey of models, analysis tools and compensation methods for the control of machines with friction," *Automatica*, vol. 30, no. 7, pp. 1083–1138, 1994.

[2] C. C. De Wit, H. Olsson, K. J. Astrom, and P. Lischinsky, "A new model for control of systems with friction," *IEEE Transactions on Automatic Control*, vol. 40, no. 3, pp. 419–425, 1995.

[3] V. Van Geffen, "A study of friction models and friction compensation," 2009.

[4] D. Won, W. Kim, D. Shin, and C. C. Chung, "High-gain disturbance observer-based backstepping control with output tracking error constraint for electro-hydraulic systems," *IEEE Transactions on Control Systems Technology*, vol. 23, no. 2, pp. 787–795, 2014.

[5] S. K. Kommuri, J. J. Rath, and K. C. Veluvolu, "Sliding-mode-based observer–controller structure for fault-resilient control in dc servomotors," *IEEE Transactions on Industrial Electronics*, vol. 65, no. 1, pp. 918–929, 2018.

[6] Z. Li, C. Su, L. Wang, Z. Chen, and T. Chai, "Nonlinear disturbance observer-based control design for a robotic exoskeleton incorporating fuzzy approximation," *IEEE Transactions on Industrial Electronics*, vol. 62, no. 9, pp. 5763–5775, 2015.

[7] J. Yao, Z. Jiao, and D. Ma, "Extended-state-observer-based output feedback nonlinear robust control of hydraulic systems with backstepping," *IEEE Transactions on Industrial Electronics*, vol. 61, no. 11, pp. 6285–6293, 2014.

[8] C. Ren, X. Li, X. Yang, and S. Ma, "Extended state observer-based sliding mode control of an omnidirectional mobile robot with friction compensation," *IEEE Transactions on Industrial Electronics*, vol. 66, no. 12, pp. 9480–9489, 2019.

[9] M. Naghdi and M. A. Sadrnia, "A novel fuzzy extended state observer," *ISA Transactions*, 2019.

[10] C. Luo, J. Yao, and J. Gu, "Extended-state-observer-based output feedback adaptive control of hydraulic system with continuous friction compensation," *Journal of the Franklin Institute*, vol. 356, no. 15, pp. 8414–8437, 2019.

[11] X. Liu, H. Cao, W. Wei, J. Wu, B. Li, and Y. Huang, "A practical precision control method base on linear extended state observer and friction feedforward of permanent magnet linear synchronous motor," *IEEE Access*, vol. 8, pp. 68 226–68 238, 2020.

[12] R. Garrido and E. Flores, "Nonlinear uncertain servomechanism tracking using an integral observer," in *2007 4th International Conference on Electrical and Electronics Engineering*. IEEE, 2007, pp. 266–269.

[13] R. R. Selmic and F. L. Lewis, "Neural-network approximation of piecewise continuous functions: application to friction compensation," *IEEE Transactions on Neural Networks*, vol. 13, no. 3, pp. 745–751, 2002.

[14] J. T. Teeter, M.-y. Chow, and J. J. Brickley, "A novel fuzzy friction compensation approach to improve the performance of a dc motor control system," *IEEE Transactions on Industrial Electronics*, vol. 43, no. 1, pp. 113–120, 1996.

[15] D. Bi, Y. Li, S. Tso, and G. Wang, "Friction modeling and compensation for haptic display based on support vector machine," *IEEE Transactions on Industrial Electronics*, vol. 51, no. 2, pp. 491–500, 2004.

[16] X. Zhou, B. Zhao, W. Liu, H. Yue, R. Yu, and Y. Zhao, "A compound scheme on parameters identification and adaptive compensation of nonlinear friction disturbance for the aerial inertially stabilized platform," *ISA Transactions*, vol. 67, pp. 293–305, 2017.

[17] C. Ahn, H. Peng, and H. E. Tseng, "Estimation of road friction for enhanced active safety systems: Algebraic approach," in *2009 American control conference*. IEEE, 2009, pp. 1104–1109.

[18] C. Makkar, W. Dixon, W. Sawyer, and G. Hu, "A new continuously differentiable friction model for control systems design," in *Proceedings, 2005 IEEE/ASME International Conference on Advanced Intelligent Mechatronics.* IEEE, 2005, pp. 600–605.

[19] M. R. Sobczyk, V. I. Gervini, E. A. Perondi, and M. A. Cunha, "A continuous version of the lugre friction model applied to the adaptive control of a pneumatic servo system," *Journal of the Franklin Institute*, vol. 353, no. 13, pp. 3021–3039, 2016.

[20] S. Wang, H. Yu, and J. Yu, "Robust adaptive tracking control for servo mechanisms with continuous friction compensation," *Control Engineering Practice*, vol. 87, pp. 76–82, 2019.

[21] S. Thenozhi, A. Concha, and J. R. Resendiz, "A contraction theory-based tracking control design with friction identification and compensation," *IEEE Transactions on Industrial Electronics*, pp. 1–10, 2021, DOI: 10.1109/TIE.2021.3094456.

[22] O. Nelles, *Nonlinear system identification: from classical approaches to neural networks and fuzzy models*. Springer Science & Business Media, 2013.

[23] J.-J. E. Slotine, W. Li *et al.*, *Applied nonlinear control*. Prentice hall Englewood Cliffs, NJ, 1991, vol. 199, no. 1.

[24] T. F. Coleman and Y. Li, "On the convergence of interior-reflective newton methods for nonlinear minimization subject to bounds," *Mathematical programming*, vol. 67, no. 1-3, pp. 189–224, 1994.

[25] M. K. Cılız and M. Tomizuka, "Friction modelling and compensation for motion control using hybrid neural network models," *Engineering Applications of Artificial Intelligence*, vol. 20, no. 7, pp. 898–911, 2007.

[26] Y.-X. Yuan, "Trust region algorithms for nonlinear programming," *Contemporary Mathematics*, vol. 163, pp. 205–205, 1994.